Electrical and morphological factors influencing the depolarizing after-potential in rat and lizard myelinated axons

Gavriel David, Barbara Modney, Karen A. Scappaticci, John N. Barrett and Ellen F. Barrett*

Department of Physiology and Biophysics, University of Miami School of Medicine, PO Box 016430, Miami, FL 33101, USA

1. Intra-axonal recording and electron microscopy were applied to intramuscular myelinated axons in lizards and rats to investigate factors that influence the amplitude and time course of the depolarizing after-potential.

2. Depolarizing after-potentials in lizard axons had larger peak amplitudes and longer half-decay times than those recorded in rat axons (mean values 10 mV, 35 ms in lizard; 3 mV, 11 ms in rat). These differences were not due to differences in temperature, resting potential or action potential amplitude or duration.

3. For a given axon diameter, the myelin sheath in lizard fibres was thinner and had fewer wraps than in rat fibres. There was no significant difference in myelin periodicity. Calculations suggest that the thinner myelin sheath accounts for $< 30\%$ of the difference between depolarizing after-potential amplitudes recorded in lizard and rat axons.

4. Consistent with a passive charging model for the depolarizing after-potential, the half-time of the passive voltage transient following intra-axonal injection of current was shorter in rat than in lizard axons.

5. Aminopyridines prolonged the falling phase of the action potential and increased the amplitude of the depolarizing after-potential in both types of axon.

6. During repetitive stimulation the depolarizing after-potentials following successive action potentials exhibited little or no summation. Axonal input conductance in the interspike interval increased during the train.

7. These findings suggest that the amplitude and time course of the depolarizing after-potential are influenced not only by the passive properties of the axon and myelin sheath, but also by persisting activation of axolemmal K^+ channels following action potentials.

In vertebrate myelinated axons, the action potential is followed by a depolarizing after-potential, which is associated with axonal superexcitability (Gasser & Erlanger, 1930; Gasser & Grundfest, 1936; Bowe, Kocsis & Waxman, 1987). There is evidence that this depolarizing after-potential arises via the following passive charging mechanism (Barrett & Barrett, 1982; Blight, 1985). During the depolarizing phase of the action potential, some current exits the axon in the internode via a leakage pathway through or under the myelin sheath. This current depolarizes (i.e. reduces the charge across) the capacitance of the internodal axolemma. When the nodal inward current terminates, a depolarizing after-potential persists until the charge across this capacitance returns to its resting value.

The mean depolarizing after-potential recorded in lizard intramuscular axons has a peak amplitude of ~10 mV and a duration of ~100 ms (Barrett & Barrett, 1982), whereas the depolarizing after-potentials recorded in rat sciatic and spinal root and cat dorsal column axons are smaller and shorter, sometimes not even detectable unless the axon is hyperpolarized by passing current (Kocsis & Waxman, 1981; Blight & Someya, 1985; Baker, Bostock, Grafe & Martius, 1987). To learn more about mechanisms underlying the depolarizing after-potential, the studies described here investigated various morphological and electrical factors that might influence its amplitude and time course. We asked whether the marked interspecies difference in after-potentials, and the changes in depolarizing after-

* To whom correspondence should be addressed.

potentials during repetitive stimulation, could be adequately explained by the above-described passive discharge model, or whether additional active currents needed to be considered as well.

We found that significant differences between lizard and rat depolarizing after-potentials persisted when recordings were made from comparable axonal locations (large axons coursing through muscle), and when resting potentials and action potentials were similar. Analysis of electron micrographs and passive voltage transients indicated that lizard axons have thinner myelin sheaths and a larger resting axolemmal resistance, which (according to the passive charging model) would contribute to the larger, longer depolarizing after-potentials recorded in lizard axons. However, the observations that K^+ channel blockers increase components of the depolarizing after-potential, and that axonal input conductance during the depolarizing after-potential increases with repetitive stimulation, suggest that K^+ conductances activated following the action potential reduce the amplitude and time course of the depolarizing after-potential, especially in rat axons.

METHODS

Preparation

The experiments used axons innervating the ceratomandibularis muscle of lizards (*Anolis sagrei*), and the diaphragm muscle of adult (3- to 5-month-old) Sprague–Dawley rats, prepared as described in David, Barrett & Barrett (1992, 1993). Both preparations permit recording from large, visualized myelinated axons, most of which are motor. Lizards were killed by decapitation followed by destruction of the brain; rats were killed by inhalation of an air–ether mixture. Dissected nerve–muscle preparations were pinned to the bottom of a Sylgard-coated chamber and perfused with physiological saline (lizard (mM): 157 NaCl, 4 KCl, 2 $CaCl_2$, 2 $MgCl_2$, 5 glucose, 1 Pipes buffer; rat (mM): 118 NaCl, 25 $NaHCO_3$, 3 KCl, 1·5 $CaCl_2$, 1 $MgCl_2$, 10 glucose, saturated with a 95% O_2–5% CO_2 mixture). In rat axons the divalent cation concentration was often increased by adding 1 mM $MnCl_2$ or by increasing Ca^{2+} to 2·5 mM, to increase the stability of intra-axonal recordings. The pH of all solutions was maintained in the range 7·2–7·5, monitored using the indicator dye Phenol Red (5 mg l^{-1}). The bathing solution was circulated using a Gilson peristaltic pump (Villiers Le Bel, France). Recordings from lizard axons were made at room temperature (19–23 °C), within the physiological operating range for this poikilothermic animal. Recordings from rat fibres were made over the range 20–31 °C, enabling comparison with lizard fibres at the lower temperatures, and approaching the physiological operating range at the higher temperatures.

Action potentials were evoked at frequencies of 0·1–50 Hz by applying brief (40–100 μs), suprathreshold depolarizing pulses to the proximal nerve trunk via a suction electrode. Muscle contractions were prevented by adding 100–300 μM carbachol to the perfusing solution.

All reagents were purchased from Sigma.

Electrophysiological recordings

Individual nerve fibres were visualized using an upright microscope (Jena, Reichert, Austria) equipped with a ×32 objective. Axons were impaled in an internodal region using microelectrodes constructed using a Brown–Flaming puller (Sutter Instrument Co., San Francisco, CA, USA) and filled with 0·2–0·5 M K_2SO_4. Electrode resistances ranged from 70 to 200 MΩ. A piezoelectric device was used to 'tap' the microelectrode through the myelin sheath into the axon (Barrett & Barrett, 1982). Intra-axonal recordings were accepted for analysis if resting potentials were −70 mV or more negative, and peak action potential amplitudes were ⩾ 70 mV. Electrophysiological recordings were limited to the larger axons, since stable intra-axonal recordings could only rarely be obtained from fibres with external (axon plus myelin) diameters smaller than 10 μm (axon diameter about 7 μm). Stable impalements were much more easily obtained in lizard than in rat axons. It was occasionally possible to insert separate current-passing and voltage-recording electrodes into the same lizard axon (as in Barrett, Morita & Scappaticci, 1988). Impalement with two microelectrodes was not feasible with rat axons, so experiments requiring current injection used a bridge circuit. At the end of some experiments the motor identity of the impaled axon was confirmed by washing carbachol out of the bath and observing a muscle twitch in response to an action potential evoked by intra-axonal current injection.

Recordings used a preamplifier (Axoclamp-2A, Axon Instruments) equipped with a bridge circuit. The capacitance neutralization was adjusted by optimizing the voltage response to a square current pulse, without oscillation. Signals were displayed on a digital oscilloscope screen, recorded on videotape via a recording adaptor (sampling frequency 11–44 kHz; model 4000A PCM, Vetter Co., Rebersburg, PA, USA) and later converted to analog form and redigitized (20–50 kHz) for computer-assisted analysis of action potentials, after-potentials, and the transient response to injected current. Slow changes in resting potential were monitored using a Gould 2200S chart recorder. Due to the high electrode-tip resistance, which often increased during passage through the connective tissue and myelin sheath surrounding the axon, high-frequency signals such as the action potential were attenuated, but slow after-potentials were faithfully recorded. Only a small subset of intra-axonal electrodes was suitable for passing current, and current amplitudes were limited to 1 nA or less. Recordings made using a bridge circuit may have distorted the more rapid components of the axonal passive response.

Morphological analyses

Measurements of fibre diameter (axon plus myelin) in fresh (non-fixed) tissue were made on small nerve bundles dissected from the muscle and placed on a glass coverslip in physiological saline. Axons prepared in this manner were well preserved, as judged by the presence of an intact perineurial sheath and a narrow (< 2 μm) nodal gap, and the absence of myelin beading or prominent clefts of Schmidt–Lanterman. External diameters of all clearly visible axons were measured from images collected with a video camera using a ×100 oil-immersion objective (Image-1 software, Universal Imaging Corp., Media, PA, USA); this technique underestimates the number of the smallest myelinated axons.

Electron micrographs were prepared by fixing the tissue for 1 h in a solution of 1·6% glutaraldehye, 0·8% paraformaldehyde in 0·1 M cacodylate buffer at pH 7·4. Following three buffer rinses the

tissue was post-fixed with 1% osmium in cacodylate buffer. The tissue was then rinsed in buffer, dehydrated in a graded ethanol series and embedded in Epon. Semi-thin sections were cut, heat-mounted on glass slides and stained with Toluidine Blue to ensure that cross-sections included the nerve. Thin sections were cut, mounted on 200-mesh copper grids and stained with lead citrate. Sections were examined and photographed with a Phillips 300 electron microscope at × 2900–46 000.

Internal axon diameter was calculated by dividing the axolemmal circumference (measured with Image-1 software from digitized, low-magnification electron micrograph negatives) by π, as suggested by Friede & Samorajski (1967). The thickness of the myelin sheath and the number of myelin wraps (counted as the number of major dense lines) were measured from high-magnification electron micrographs using a microscope equipped with a camera lucida; each recorded thickness was the mean of three to four measurements made for each sheath. Excluded from these measurements were axons cross-sectioned through the node or paranode region, and sheaths in which the myelin wraps were split due to fixation artifacts.

Data are given as means ± S.D., and the significance of differences between measurements in lizard and rat fibres was determined using Student's unpaired t test. Regression lines were fitted and correlation coefficients calculated using CoPlot (Cohort Software, Berkeley, CA, USA). The significance of differences between regression lines was determined as described in Glantz & Slinker (1990).

RESULTS

Intra-axonal recordings from lizard and rat intramuscular fibres

Figure 1 shows representative action potentials (*A*) and depolarizing after-potentials (*B*) recorded intra-axonally following suprathreshold stimulation of the proximal nerve trunk in a lizard (left) and a rat (centre) intramuscular axon. Action potential amplitudes were similar in the two preparations. The shorter duration of the rat action potential is attributable at least in part to the higher temperature of the rat recording (25 °C, compared with 19 °C for lizard), since in rat axons over the range 20–31 °C, action potential duration at half-amplitude decreased as the temperature increased ($r = -0{\cdot}84$, $P < 0{\cdot}001$). The depolarizing after-potential was larger and longer in the lizard axon.

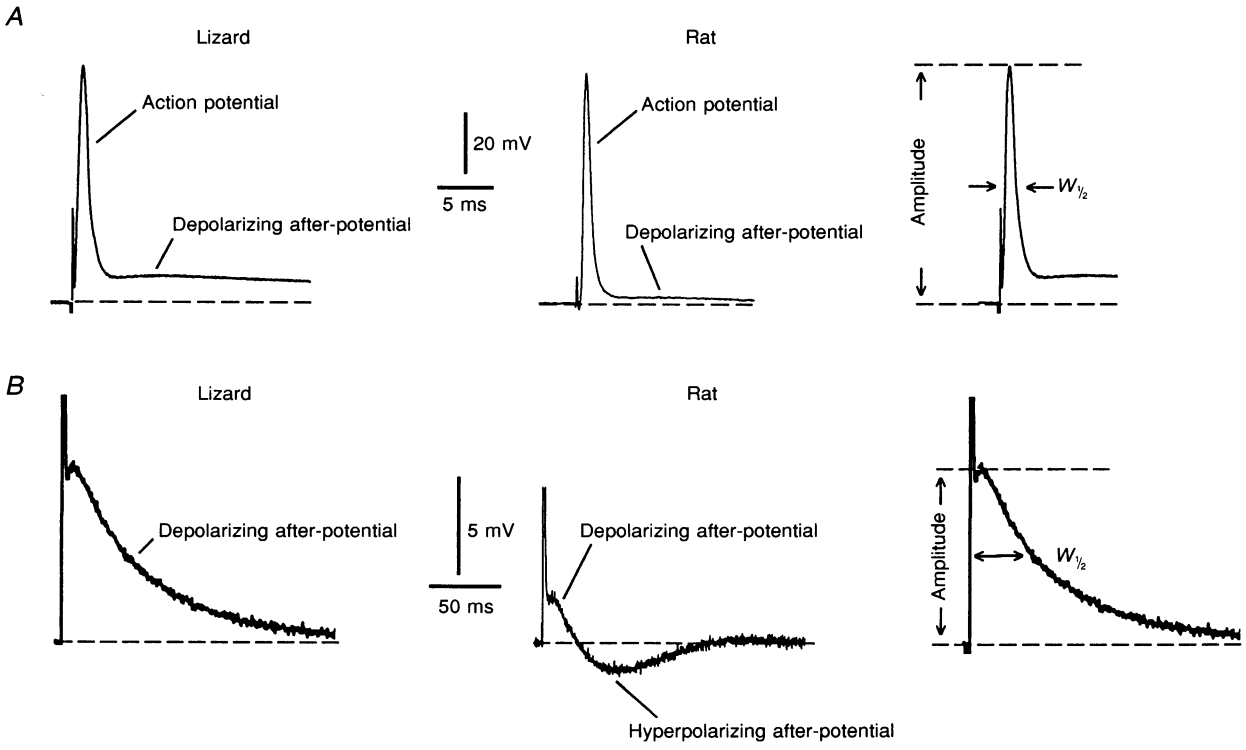

Figure 1. Intra-axonal recordings from lizard ceratomandibularis (left) and rat diaphragm (centre) motor axons

A, action potentials and depolarizing after-potentials evoked by stimulating the proximal nerve trunk. *B*, slower, higher-gain traces from the same axons, illustrating the full time course of the depolarizing and (in rat) hyperpolarizing after-potentials (action potential peaks are truncated). Dashed lines indicate resting potentials (−82 mV for lizard, −77 mV for rat). Recording temperatures were 19 °C for lizard, 25 °C for rat. The insets on the right demonstrate methods of measuring the peak amplitudes and durations at half-peak amplitude ($W_{½}$) given in Table 1.

Table 1. Potentials measured in lizard and rat motor axons

	Lizard	Rat
Resting potential (mV)*	78·0 ± 4·7	74·4 ± 3·7
Action potential		
Amplitude (mV)	81·2 ± 14·3	74·9 ± 8·7
Duration (m)	0·90 ± 0·29	0·81 ± 0·28
Depolarizing after-potential		
Amplitude (mV)**	10·0 ± 3·8	2·84 ± 2·6
Duration (ms)**	34·8 ± 13·6	11·2 ± 4·6
Hyperpolarizing after-potential		
Amplitude (mV)	n.d.	0·62 ± 0·55

Values are means ± S.D. for $n = 21$ (lizard) and $n = 20$ (rat) axons. Peak amplitude and duration at half-peak amplitude ($W_{½}$) were measured as indicated in Fig. 1 insets. (In records where there was no distinct break between the action potential and the depolarizing after-potential (e.g. Figs 5*A* and 7), the amplitude of the depolarizing after-potential was measured at the intersection of a line extrapolated from the slow component of the depolarizing after-potential and a line extrapolated from the steepest portion of the falling phase of the action potential.) Single and double asterisks indicate significant difference between lizard and rat axons at $P < 0·01$ and $P < 0·001$, respectively. Temperatures were 20·2 ± 0·9 °C for lizard, and 25·4 ± 3·6 °C for rat. n.d., not detected.

Table 1 presents mean values of resting potentials and amplitudes and durations of action potentials and depolarizing after-potentials from twenty-one lizard and twenty rat axons. There was no significant difference between lizard and rat axons with regard to peak amplitude or duration (at half-peak amplitude) of the action potential, but the mean resting potential in rat axons was slightly more depolarized than that in lizard axons. The depolarizing after-potential in rat axons was significantly smaller and shorter than that in lizard axons. These differences in depolarizing after-potential amplitude and duration persisted ($P < 0·001$) when the temperatures of both preparations were equal (19–23 °C).

These results demonstrate that the depolarizing after-potentials recorded in rat and lizard axons have different amplitudes and time courses even when recordings are made in comparable locations (intramuscular axons) and at similar temperatures with similar action potential amplitudes and durations. The slightly (3·6 mV) more depolarized mean resting potential in the sampled rat axons may have contributed to their smaller depolarizing after-potential, but the data of Fig. 5*C* suggest that this contribution was small, accounting for no more than 1 mV of the 7·2 mV difference between the mean amplitudes recorded in rat and lizard axons.

A hyperpolarizing after-potential followed the depolarizing after-potential in rat, but not in lizard, axons. The peak amplitude of this hyperpolarizing after-potential was 0·62 ± 0·55 mV ($n = 20$). A similar slowly developing hyperpolarizing after-potential was seen in extracellular whole-nerve recordings from mammalian A fibres (Gasser & Grundfest, 1936) and in individual rat sciatic and ventral root axons by Baker *et al.* (1987) and Eng, Gordon, Kocsis & Waxman (1988). This after-potential appears to be produced by a tetraethylammonium (TEA)-sensitive, non-Ca^{2+}-dependent K^+ conductance (Eng *et al.* 1988).

Dimensions of nerve fibres

Distribution of fibre diameters in fresh tissue

Figure 2 shows the distribution of outer fibre diameters (axon + sheath) measured in an unfixed population of 129 lizard and 104 rat fibres readily visible with the light microscope. In this population, lizard fibres had a significantly larger mean diameter than rat fibres (lizard, 9·80 ± 1·76 μm; rat, 7·69 ± 1·16 μm, $P < 0·001$). This difference is in a direction opposite to that expected from the observed difference in depolarizing after-potential amplitude, since the passive discharge model predicts (all else being equal) that larger axons should have smaller depolarizing after-potentials. These measurements of fibre diameter in fresh tissue underestimate the number of small myelinated axons, but give a reasonable representation of the larger fibres accessible to intra-axonal electrophysiological recording.

Axon diameter, myelin sheath thickness and myelin periodicity in fixed tissue

Electron micrographs of intramuscular axons were used to determine whether the larger mean outer diameter of lizard axons was due primarily to a larger axonal diameter and/or to a larger myelin sheath diameter.

Figure 3 shows electron micrograph cross-sections of lizard and rat intramuscular nerve bundles; the insets show higher magnification sections used to count the number of myelin wraps. Figure 4 summarizes the measurements made from a sample of micrographs. Figure 4*A* shows the distribution of diameters of lizard and rat myelinated axons; these distributions were not significantly different (mean for lizard: 5·96 ± 3·00 μm, $n = 80$; for rat:

5·09 ± 1·49 μm, $n = 138$); the lizard distribution appeared bimodal. If one considers only those axons likely to be detected in fresh tissue by light microscopy (outer diameters of 4 μm or more (Fig. 2), corresponding to axonal diameters of 3 μm or more), then the mean diameter in this subset of rat axons (5·4 ± 1·2 μm, $n = 122$) was significantly smaller than that in the subset of lizard axons (7·0 ± 2·6 μm, $n = 63$, $P < 0·001$). The lizard motor nerve also contained proportionally more axons with diameters >7 μm, suitable for intra-axonal electrophysiological recording.

Figure 4*B* plots the ratio (d/D) of axonal diameter (d) to outer fibre diameter (D) where $D = d + (2 \times$ myelin sheath thickness) as a function of d. Regression lines fitted to these data (not shown) indicated a moderate increase in d/D with increasing d in both lizard and rat axons; the slopes of these lines were not significantly different. Measured d/D values ranged from 0·60 to 0·87, comparable with reported values of 0·76 for cat motor fibres (Quick, Kennedy & Donaldson, 1979) and 0·6–0·8 for mouse sciatic axons (Friede & Samorajski, 1967).

Figure 4*C* shows that the number of myelin wraps increased linearly with myelin thickness in both rat and lizard preparations. The slopes of fitted regression lines (not shown) were not significantly different, indicating that the myelin periodicity in these rat and lizard axons was similar. These measurements yielded values of 15·6–16·7 nm per myelin wrap. For comparison, Peters, Palay & Webster's (1991) analysis of fixed and embedded peripheral nerves yielded a value of 12 nm, and Kirschner, Ganser & Caspar's (1984) analysis of wide-angle X-ray diffraction of fresh mouse sciatic nerves yielded values of 17·0–18·5 nm per wrap.

Figure 4*D* plots the relationship between myelin sheath thickness and axon diameter for rat and lizard fibres. Myelin sheath thickness increased with axon diameter in both groups (correlation coefficients for fitted regression lines were 0·86 for lizard and 0·76 for rat), compatible with similar findings reported for myelinated axons in mouse sciatic nerve (Friede & Samorajski, 1967), cat spinal cord (Hildebrand, 1971) and rabbit gastrocnemius nerve (Williams & Wendell-Smith, 1960). For a given increase in axon diameter, the increase in myelin sheath thickness was ~30% larger for rat than for lizard axons ($P < 0·001$).

These electron micrographic studies indicate that for the intra-muscular nerve bundles studied here, lizards have more large axons, and those large axons have thinner myelin sheaths, than those measured (or extrapolated) for comparably sized rat axons. This finding helps explain why this lizard preparation has been especially favourable for intra-axonal recording. The similar myelin periodicity in lizard and rat axons suggests that one species does not have more 'loosely packed' myelin than the other. Assuming that thinner (fewer wraps) myelin sheaths offer less resistance to trans-internodal current than thicker myelin sheaths, and that the depolarizing after-potential involves passive charging, the observation of a smaller myelin sheath : axon diameter ratio in lizard axons is in the right direction to explain the larger depolarizing after-potentials recorded in lizard axons. This possibility is considered quantitatively in simulations presented in the Discussion.

Voltage dependence of passive voltage response and depolarizing after-potential

If the depolarizing after-potential is indeed a passive discharge, then one would expect that the faster depolarizing after-potential recorded in rat axons would be

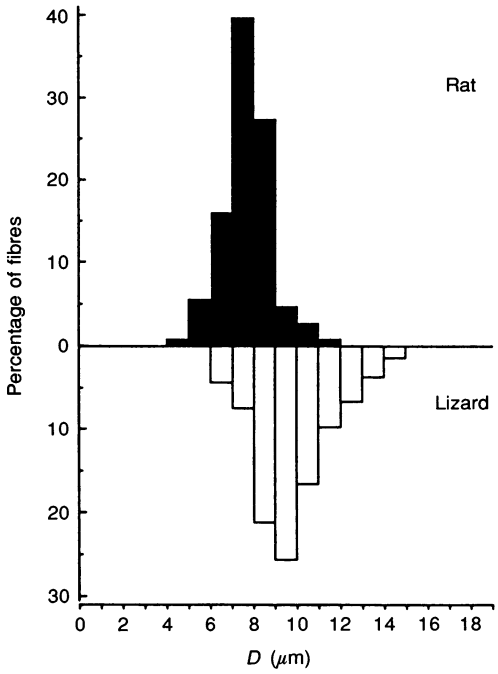

Figure 2. Histograms of external fibre diameters measured at ×100 magnification from freshly dissected rat and lizard motor nerve fibres in physiological saline

Rat data (■) were measured from 104 fibres in 2 preparations; lizard data (□) from 129 fibres in 3 preparations. D, external fibre diameter (axon plus myelin).

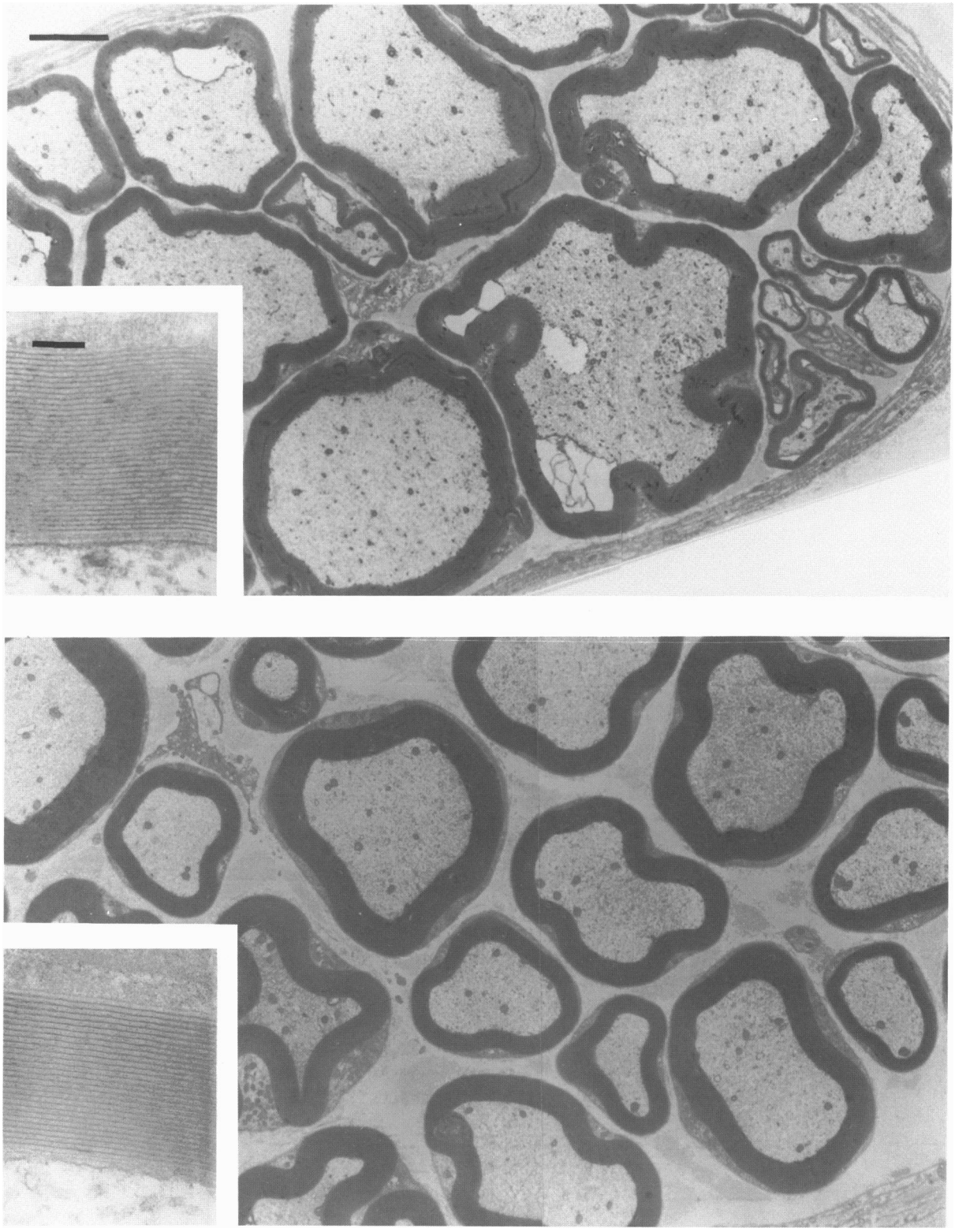

Figure 3. Montage of electron micrographs of cross-sections through fixed and embedded lizard (upper) and rat (lower) motor nerve bundles

Insets at left show at higher magnification representative sections through compact myelin from different fields. Calibration bars (3 μm and 0·2 μm in inset) apply to both lizard and rat fibres.

accompanied by an input resistance smaller than, and a passive voltage transient faster than, those recorded in lizard axons. Figure 5 shows superimposed voltage transients evoked in a rat (*A*) and a lizard (*B*) axon by intra-axonally injected current pulses. These traces also show depolarizing after-potentials following action potentials evoked by stimulating the proximal nerve trunk during the current pulses. Figure 5*C* compares the steady-state current–voltage relationships obtained from records like those in parts *A* and *B*. Both curves exhibit outward rectification. At hyperpolarized potentials the chord resistance was 29 MΩ in the rat, and 89 MΩ in the lizard axon. In a sample of rat axons the mean chord resistance at hyperpolarized potentials was 45 ± 47 MΩ (range, 4·2–160 MΩ, $n = 9$). The comparable chord resistances in lizard axons were larger (96 ± 45 MΩ, range, 34–150 MΩ, $n = 8$, $P < 0{\cdot}05$; see also current–voltage relationships in Barrett & Barrett, 1982; Barrett *et al.* 1988).

Figure 5*D* shows that in both lizard and rat axons the peak amplitude of the depolarizing after-potential varied approximately linearly with membrane potential. The slope of the best-fitting line (change in depolarizing after-potential amplitude : change in membrane potential) was −0·27 in the rat, and −0·75 in the lizard axon. In a sample of rat axons the mean slope was −0·38 ± 0·13 (range, −0·58 to −0·26, $n = 5$), significantly different from the mean slope in lizard axons (−0·74 ± 0·22; range, −1·08 to −0·47, $n = 9$, $P < 0{\cdot}01$; see also Barrett & Barrett, 1982; Barrett *et al.* 1988; Morita, David, Barrett & Barrett, 1993). Figure 5*E* and *F* shows how the rates of decay of the depolarizing after-potential (●) and the passive voltage response to applied current pulses (△) varied as a function of the final membrane potential in a rat (*D*) and a lizard (*E*) axon. Over this range of membrane potentials the rates of decay were faster in rat than in lizard axons: in rat axons the slowest passive time constant at the resting potential

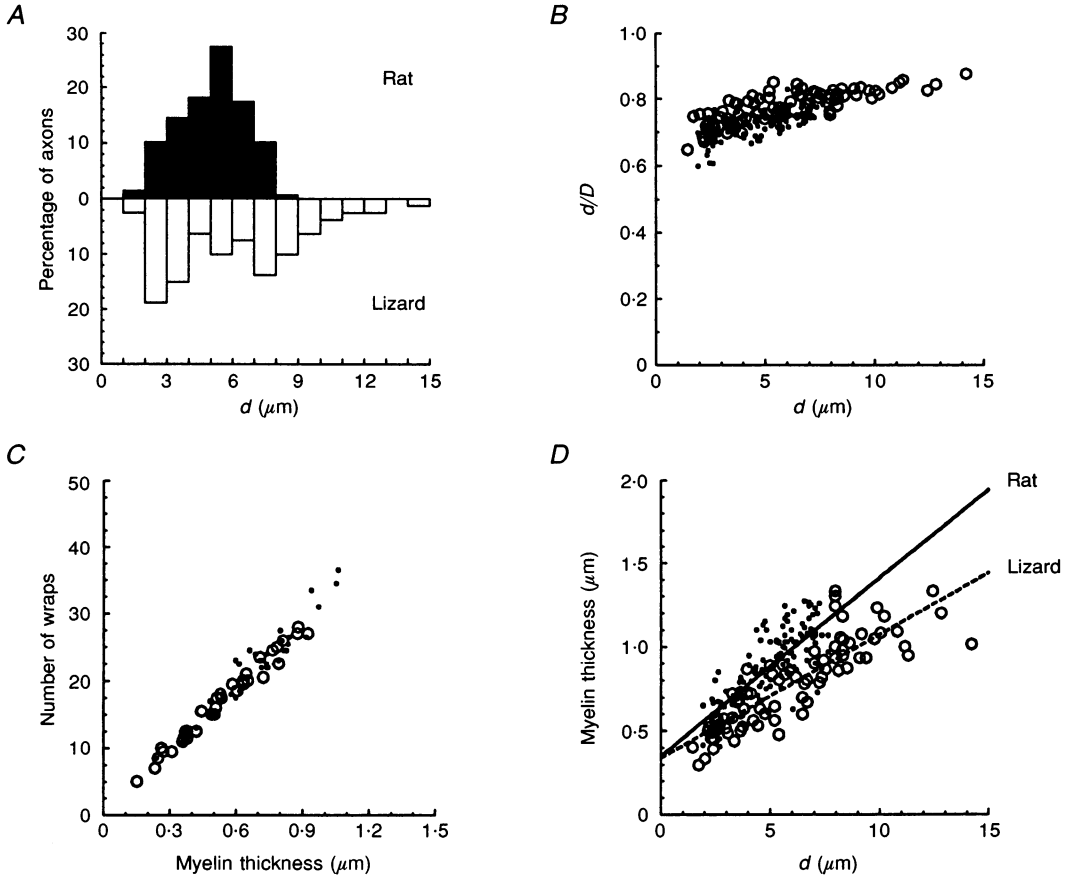

Figure 4. Dimensions of axons and myelin sheaths measured from digitized electron micrographs

A, histogram of axonal diameters (d) of myelinated fibres (rat, ■; lizard, □), measured by dividing the circumference by π. *B*, ratio of axonal diameter (d) to outer fibre diameter (D), where $D = d + (2 \times$ myelin thickness), as a function of d. *C*, number of myelin wraps as a function of myelin thickness. Rat and lizard axons averaged 64 ± 3·2 and 59·8 ± 1·49 myelin wraps (μm myelin sheath)$^{-1}$, respectively; these values were not significantly different. *D*, myelin thickness as a function of d. In *B*, *C* and *D*, ● refers to rat fibres and ○ to lizard. The slopes of the regression lines fitted to these data were 0·106 ± 0·008 μm myelin (μm axon)$^{-1}$ for rat, and 0·0735 ± 0·0050 μm myelin (μm axon)$^{-1}$ for lizard; $P < 0{\cdot}001$.

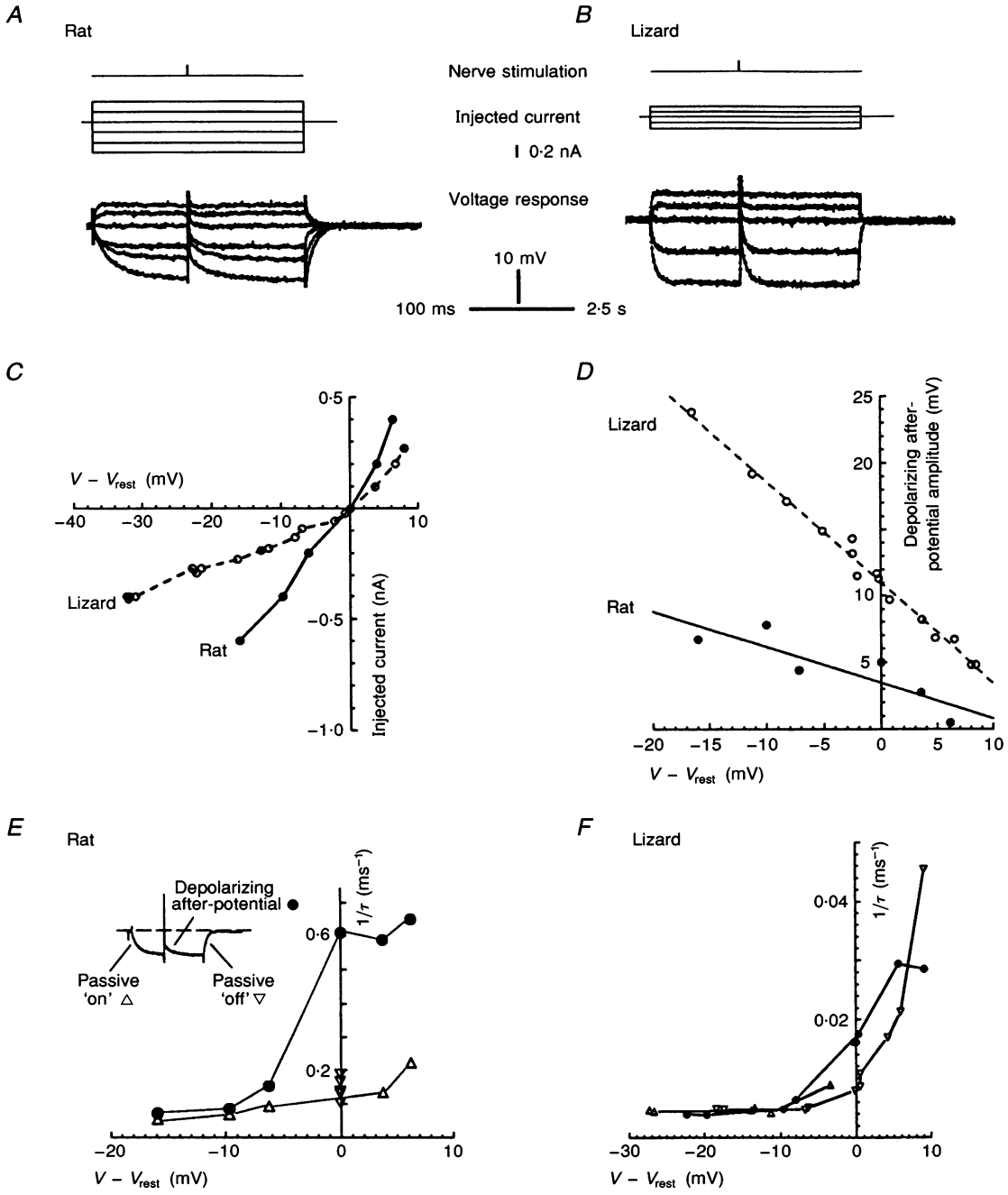

Figure 5. Passive voltage transients and depolarizing after-potentials in rat and lizard axons

A and *B*, passive voltage transients evoked by the indicated intra-axonally injected current pulses in a rat (*A*) and a lizard (*B*) axon. During the pulse an action potential was evoked by stimulating the proximal nerve trunk. Note that the time scale represents 100 ms for rat, and 2·5 s for lizard records. Current was injected into the rat axon via a bridge circuit (−0·6 to +0·4 nA, 200 ms), and into the lizard axon via a second intra-axonal electrode (−0·23 to +0·20 nA, 5 s). *C*, current–voltage relationships measured in the rat axon of *A* (●) and the lizard axon of *B* (○). *D*, peak amplitude of the depolarizing after-potential as a function of membrane potential displacement in the rat and lizard axons of *A* and *B*. Best-fit regression lines are shown. *E* and *F*, reciprocal of the slowest time constant of decay ($1/\tau$) of the depolarizing after-potential (●) and the passive on (△) and off (▽) voltage transients in rat (*E*) and lizard (*F*) axon as a function of steady-state membrane potential displacement (see inset in *E*). Rat axon same as *A*; lizard axon different from *B*. Time constants were measured from the slopes of regression lines fitted to semi-logarithmic plots. Note the different ordinate scales in *E* and *F*.

averaged 10·0 ± 6·7 ms (range, 6–20 ms, $n = 4$), whereas in lizard axons this time constant averaged 71 ± 24·5 ms (range, 34–112 ms, $n = 8$, $P < 0{\cdot}001$). The more rapid decay of the passive voltage transient in rat axons, combined with their lower mean input resistance, suggests that rat intramuscular axons have a lower axolemmal resistance than lizard intramuscular axons (see Discussion).

For both types of axon the passive voltage transient and the depolarizing after-potential had similar rates of decay at hyperpolarized potentials, compatible with the passive charging model for the depolarizing after-potential. However, at resting and depolarized potentials the depolarizing after-potential tended to decay more rapidly than the passive voltage transient, especially in rat axons. This discrepancy, along with the slow hyperpolarizing after-potential recorded in rat axons (Fig. 1*B*), suggests that axonal input conductance may remain elevated for some time following action potentials evoked from resting and depolarized membrane potentials.

Voltage trajectories during the interspike interval

Voltage trajectories recorded during repetitive discharge provide further evidence for prolonged activation of conductances following action potentials. Figure 6 (left) shows interspike voltage trajectories recorded during 50 Hz stimulation in the lizard and rat axons of Fig. 1. These trajectories resemble those obtained by extracellular whole-nerve recordings from frog and mammalian A fibres by Gasser (1935) and Gasser & Grundfest (1936). To the right of the lizard record is a simulation showing how passive depolarizing after-potentials with an amplitude and slow time constant of decay comparable to those recorded in this lizard axon (Fig. 1*B*, left) would be expected to summate during 50 Hz stimulation. (A comparable simulation could not be done in rat axons due to their hyperpolarizing after-potential.) In both lizard and rat axons the recorded depolarizing after-potentials exhibited little or no summation.

The experiment illustrated in Fig. 7 investigated whether the lack of summation of depolarizing after-potentials during repetitive stimulation was associated with an increase in axonal input conductance during the interspike interval. Trace *A* illustrates interspike voltage trajectories during 20 Hz stimulation in a lizard axon impaled with separate current-passing and voltage-recording electrodes. In trace *B* a hyperpolarizing test current pulse was injected during each interspike interval. Trace *C* shows the voltage changes produced by injecting identical hyperpolarizing current pulses into the resting axon. Compare this with trace *D*, which plots the difference between traces *A* and *B*, and thus indicates the voltage changes produced by current pulses injected during the train. The voltage transient following the first action potential was similar to that recorded in the resting axon, but the voltage transients following the second and subsequent impulses in the train had smaller peak amplitudes and smaller voltage × time integrals, indicating an increased axonal input conductance. This result, combined with the fact that the later interspike trajectories traversed a voltage range that was not more depolarized than the first interspike trajectory, suggests that the failure of depolarizing after-potentials to summate appreciably during repetitive stimulation is due at least in part to an increase in axonal

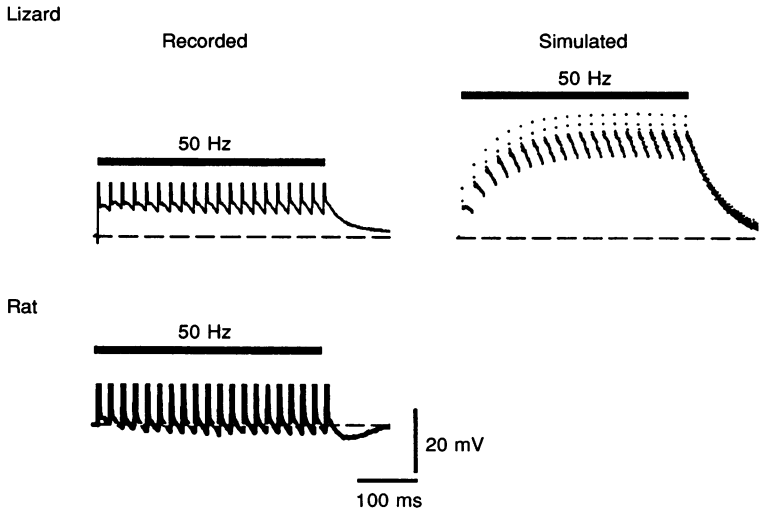

Figure 6

Traces at left show interspike voltage trajectories recorded during stimulation at 50 Hz in lizard (upper) and rat (lower) axons of Fig. 1. Action potential peaks are truncated. Trace at right shows the trajectory simulated assuming linear summation of the depolarizing after-potential recorded in the lizard axon.

input conductance that persists throughout the interspike interval.

We could not obtain comparable two-electrode recordings in rat axons, but records such as those in Figs 6 and 9*C* suggest that an even more prominent progressive increase in axonal input conductance (probably due to opening of K^+ channels) occurs in this preparation, since the membrane potential became progressively more hyperpolarized during successive interspike intervals.

If the depolarizing after-potential is indeed a passive charging phenomenon whose amplitude and time course are influenced by activation of axolemmal conductances, then one would expect that depolarizing after-potentials would summate more if activation of these extra conductances were minimized. To test this prediction, a lizard axon was stimulated repetitively at the resting potential (Fig. 8*A*) and during the passage of increasing intensities of hyperpolarizing current through the recording electrode (Fig. 8*B–D*). In trace *B* the small amplitude of the first action potential suggested that propagation was blocked at a node proximal to the recording electrode. The ensuing small depolarizing after-potential raised axonal excitability sufficiently to permit the second and all subsequent action potentials to propagate at full amplitude. With the more intense hyperpolarizing current in trace *C* the first two action potentials had amplitudes even smaller than that of the first action potential in *B*, suggesting block of propagation at a node even more distant from the recording electrode. Summation of four small depolarizing after-potentials permitted subsequent action potentials to propagate at full amplitude. In trace *D* the hyperpolarizing current was so intense that, even with summation of many small depolarizing after-potentials, no action potentials propagated at full amplitude past the recording electrode. Figure 8*E* superimposes traces *A–C* (see legend for details). The lower arrow indicates a voltage level approximating the threshold for the medium-sized action potential, and the

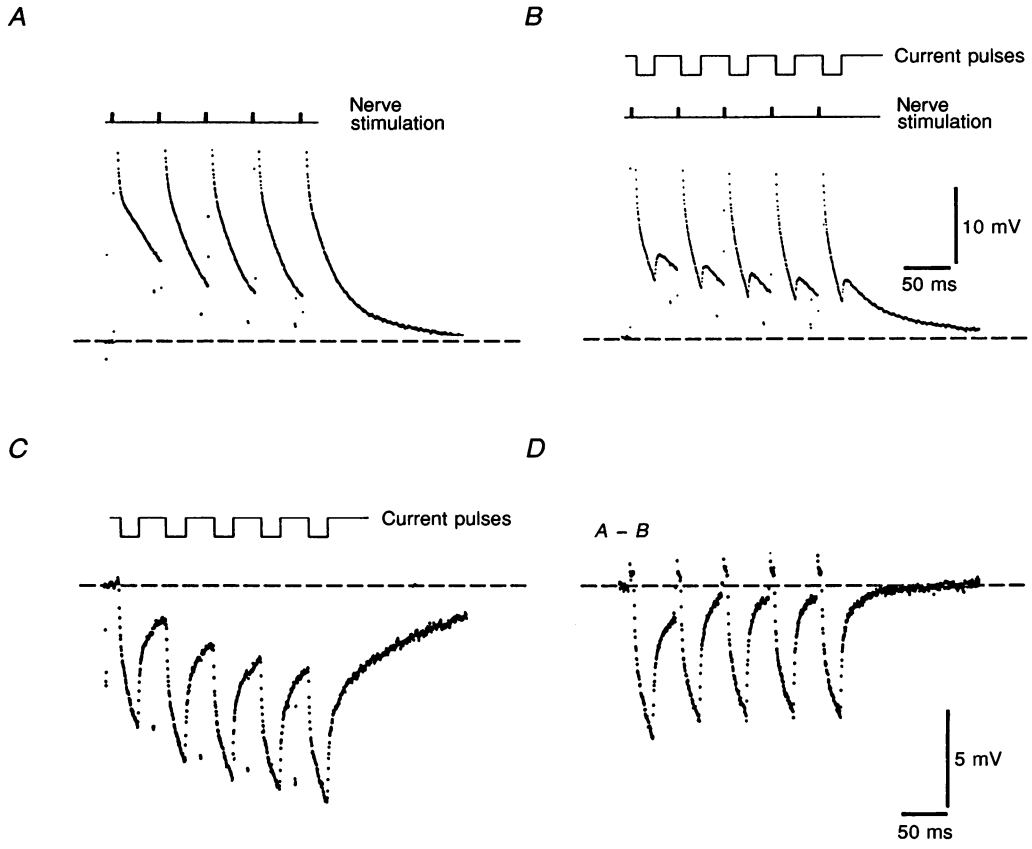

Figure 7. Interspike voltage trajectories and passive voltage transients in a lizard axon impaled with separate current-passing and voltage-recording microelectrodes and stimulated at 20 Hz via the proximal nerve trunk

A, interspike voltage trajectories. *B*, interspike voltage trajectories when hyperpolarizing current pulses (−0·5 nA, 20 ms) were injected into the axon at identical times during each interspike interval. *C*, voltage transients elicited by injecting the same current pulses into the resting axon. *D*, difference between traces *A* and *B*, representing the voltage change produced by injecting current pulses during interspike intervals. Peak amplitudes of action potentials in *A* and *B* were truncated.

upper arrow approximates the threshold for the full-sized action potential.

These data suggest that depolarizing after-potentials can summate passively until their summed depolarizations activate conductances that limit further increases in depolarizing after-potential amplitude.

Effect of K^+ channel blocking agents on the depolarizing after-potential

Nodal, paranodal and internodal axolemmae express several types of delayed-rectifier K^+ channel (rat: Baker *et al.* 1987; Eng *et al.* 1988; Röper & Schwarz, 1989; Wilson & Chiu, 1990; Safronov, Kampe & Vogel, 1993; rabbit: Chiu & Schwarz, 1987; lizard: Angaut-Petit, Benoit & Mallart, 1989; frog/toad: Dubois, 1981; Grissmer, 1986; Jonas, Bräu, Hermsteiner & Vogel, 1989; Wu, Rubinstein & Shrager, 1993). Other K^+ channels identified in axolemmal membranes include Ca^{2+}-activated and Na^+-activated channels, inwardly rectifying channels, and background channels with minimal voltage dependence (Wilson & Chiu, 1990; Jonas, Koh, Kampe, Hermsteiner & Vogel, 1991; Koh, Jonas, Bräu & Vogel, 1992; Wu *et al.* 1993; Koh, Jonas & Vogel, 1994). Activation of K^+ channels would be expected to speed the repolarization of the action potential, to reduce the voltage change produced across the internodal axolemma by a given depolarizing current, and to reduce the membrane time constant. Thus one would predict that application of K^+ channel blocking agents would increase the duration of the action potential, and increase the amplitude and slow the decay of the depolarizing after-potential. Barrett *et al.* (1988) reported that in lizard axons a 10–20 min exposure to 1 mM 4-aminopyridine (4-AP) increased action potential duration by 92% and increased the amplitude and slow time constant of decay of the depolarizing after-potential by 16 and 25%, respectively. Figure 9*A* demonstrates that in rat axons 1 mM 4-AP increased action potential duration and increased axonal depolarization during the initial portion of the depolarizing after-potential ($n = 3$). Any effect of 4-AP on the later time course of the depolarizing after-potential was obscured by enhancement by 4-AP of the subsequent hyperpolarizing after-potential (Fig. 9*B*; see

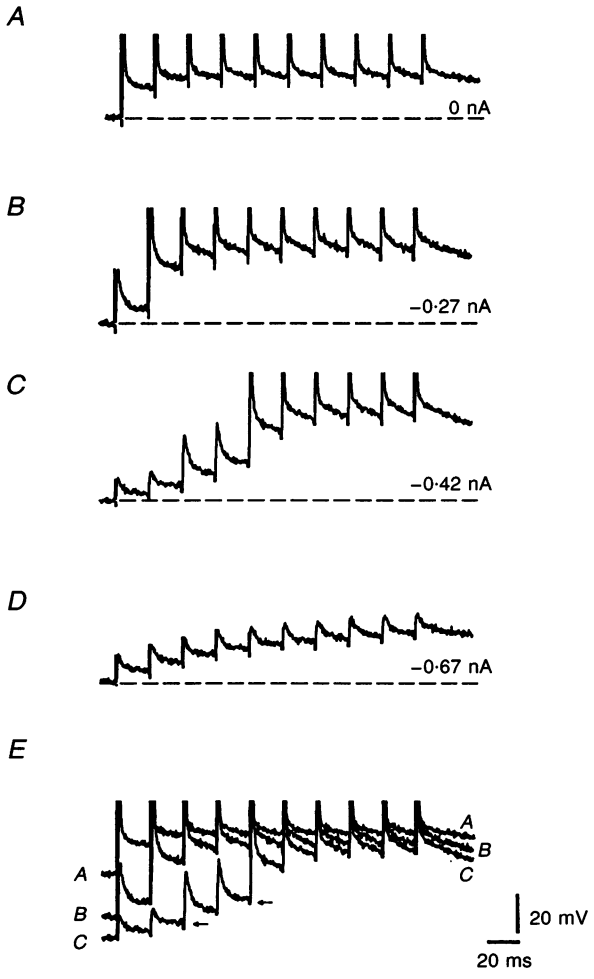

Figure 8. Summation of submaximal depolarizing after-potentials in a lizard axon during repetitive stimulation at 50 Hz

A, interspike voltage trajectories at the resting potential. *B–D*, interspike voltage trajectories obtained during similar stimulation in the presence of a steady hyperpolarizing current (−0·27, −0·42 and −0·67 nA, respectively) injected through the recording electrode. Depolarizing after-potentials following small action potentials showed more summation than those following full-sized action potentials. *E*, superimposition of traces *A*, *B* and *C*, achieved by overlapping the peak of the final action potential in each train. Due to the high input conductance at the peak of the action potential, this portion of the voltage record should be least susceptible to distortions caused by passing current through the recording electrode (although some distortion is likely for recording sites in the middle of the internode). Upper and lower arrows indicate the approximate thresholds for evoking full- and medium-amplitude action potentials, respectively. Action potentials in *A* had a peak amplitude of 90 mV; they and the full-sized action potentials in *B*, *C* and *E* were truncated.

also Baker *et al.* 1987; Eng *et al.* 1988). During repetitive stimulation in 4-AP the initial portion of the depolarizing after-potential remained more depolarized than that recorded in control solution (Fig. 9*C*).

Figure 10*A* shows that 0·1 mM 3,4-diaminopyridine (3,4-DAP) also increased action potential duration and the initial portion of the depolarizing after-potential in lizard axons. Analysis of semilogarithmic plots (not shown) indicated that in this axon 3,4-DAP increased the slowest time constant of decay from 55 ms in control solution to 80 ms, and added a prominent faster component with a time constant of 15 ms. Addition of 2 mM TEA further prolonged the action potential and the depolarizing after-potential and increased the peak amplitude of the depolarizing after-potential (see also Barrett *et al.* 1988). The increased amplitude of the depolarizing after-potential produced by these K^+ channel blockers persisted during repetitive stimulation (Fig. 10*B*).

Even though these K^+ channel blockers prolonged the decay of the depolarizing after-potential following single action potentials in lizard axons, there was little or no summation of depolarizing after-potentials during repetitive stimulation. One likely reason for this lack of summation is that these concentrations of aminopyridines and TEA blocked only a fraction of axolemmal delayed-rectifier channels, so that many K^+ channels remained available to be cumulatively activated by the more depolarized interspike potentials prevailing in the presence of these drugs. The effects of bath-applied TEA on the depolarizing after-potential develop slowly, suggesting restricted diffusional access to internodal K^+ channels (Barrett *et al.* 1988), and in demyelinated preparations internodal K^+ channels appear to be more resistant to TEA than nodal K^+ channels (Chiu & Ritchie, 1980, 1981, 1982; Chiu, Shrager & Ritchie, 1985; Grissmer, 1986). It was difficult to test higher drug concentrations, because continued exposure to 0·1 mM 3,4-DAP plus 2 mM TEA blocked conduction in the axon of Fig. 10, and lizard axons bathed in high concentrations of TEA (> 10 mM, or lower concentrations if aminopyridines are also present) exhibit prolonged plateaux after the action potential and

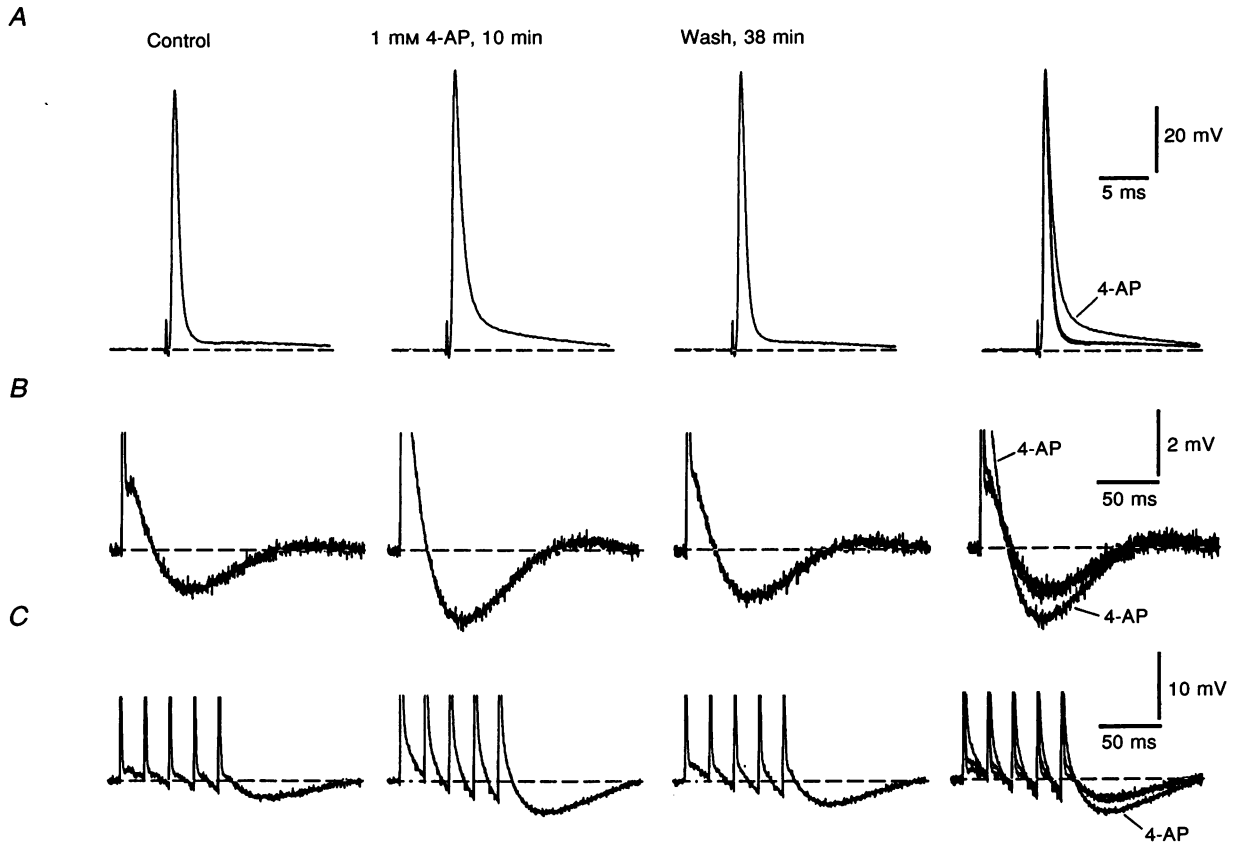

Figure 9. Effect of 4-aminopyridine (4-AP) on action potentials (*A*), after-potentials (*B*) and interspike voltage trajectories (*C*) in a rat axon stimulated at 0·5 (*A*, *B*) or 50 Hz (*C*)

Records from left to right were obtained in control solution, 10 min after addition of 1 mM 4-AP to the bath, and 38 min after return to control solution. All traces are superimposed at the far right. Resting potentials were −77 mV in control solution, −72 mV in 4-AP and −84 mV following return to control solution. Peak amplitudes of action potentials in *B* and *C* were truncated.

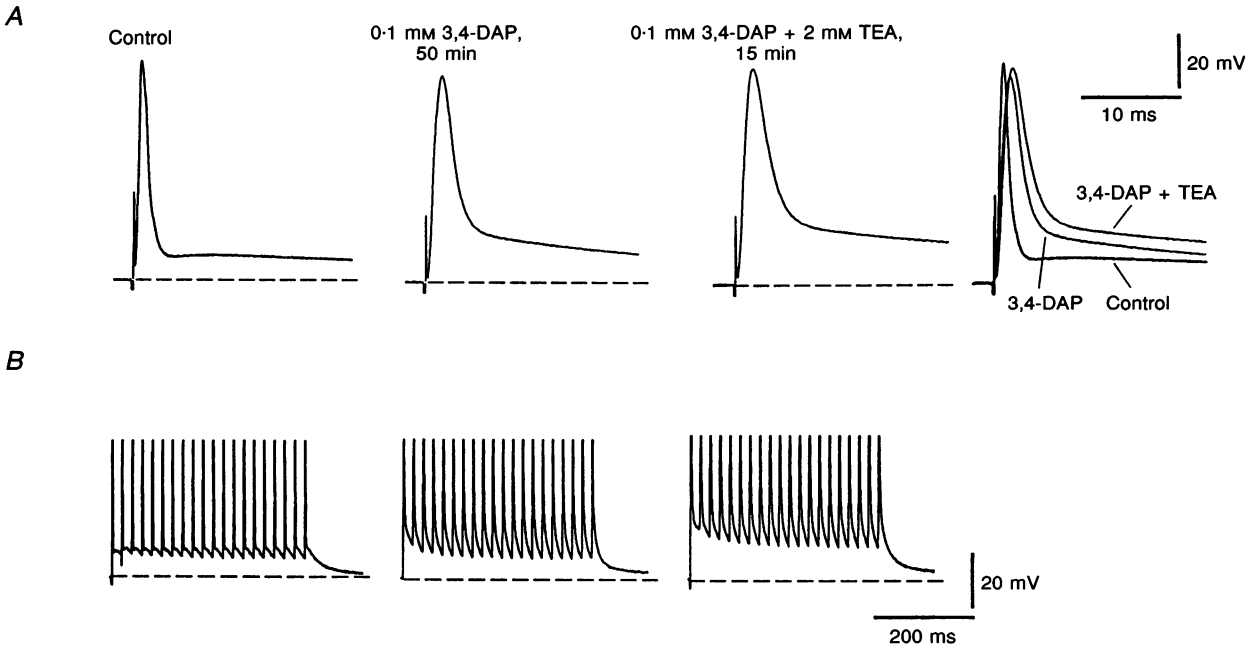

Figure 10. Effects of K^+ channel blocking agents on action potentials (*A*) and interspike voltage trajectories (*B*) during 50 Hz stimulation in a lizard axon

Records from left to right were obtained in control solution, 50 min after addition of 0·1 mM 3,4-diaminopyridine (3,4-DAP) to the bath, and 15 min after the further addition of 2 mM TEA. Records in *A* are superimposed at the far right. Longer exposure to 3,4-DAP + TEA resulted in conduction block (not shown). All solutions contained 2 mM Mn^{2+} to minimize Ca^{2+}-dependent potentials from nerve terminals (Morita & Barrett, 1989). Resting potentials were −85 mV in control, and −87 mV in both 3,4-DAP and 3,4-DAP + TEA. Peak amplitudes of action potentials in *B* were truncated.

spontaneous oscillations in resting potential (Morita & Barrett, 1989; Morita, Barrett & Katayama, 1990).

Because of these effects, and because K^+ channel blockers modify not only the depolarizing after-potential, but also the duration of the preceding action potential and (in rat axons) the amplitude of the following hyperpolarizing after-potential, it was difficult to distinguish between the indirect and direct effects of these drugs on the depolarizing after-potential and interspike voltage trajectories. However, available evidence does suggest that current through K^+ channels activated following the action potential normally limits the amplitude of the depolarizing after-potential and speeds its time course.

DISCUSSION

Experiments presented here investigated factors that influence the amplitude and time course of the depolarizing after-potential in myelinated axons. The large differences between the amplitudes and time courses of depolarizing after-potentials recorded in lizard and rat axons persisted when measurements were made in comparable intramuscular locations and at similar temperatures. Differences in resting potential and/or action potential configuration may contribute to, but cannot wholly account for, these differences. Also, there was no detectable difference in the tightness of packing of the compact myelin layers surrounding rat and lizard axons. Several factors might help account for the smaller amplitude and shorter duration of depolarizing after-potentials recorded in rat axons, including (1) a higher-resistance myelin sheath, (2) a lower resting axolemmal resistance, and (3) greater activation of axolemmal K^+ channels following action potentials. Some of these K^+ channels probably contribute to the hyperpolarizing after-potential recorded in rat axons. Cumulative activation of axolemmal conductances probably helps to account for the observation that depolarizing after-potentials exhibit little or no summation during repetitive stimulation.

Effects of myelin sheath resistance

Morphological measurements (Fig. 4*D*) indicated that rat axons tended to have thicker myelin sheaths (and more myelin wraps) than comparably sized lizard axons. We did simulations using a simplified passive charging model (Fig. 11*A*) to estimate the extent to which the rat's thicker myelin sheath might account for the smaller amplitude and/or faster time course of its depolarizing after-potential. Figure 11*B* plots the peak amplitude of the simulated depolarizing after-potential as a function of myelin resistance, R_y. The two curves were calculated using estimated maximal (●) and minimal (○) values for the

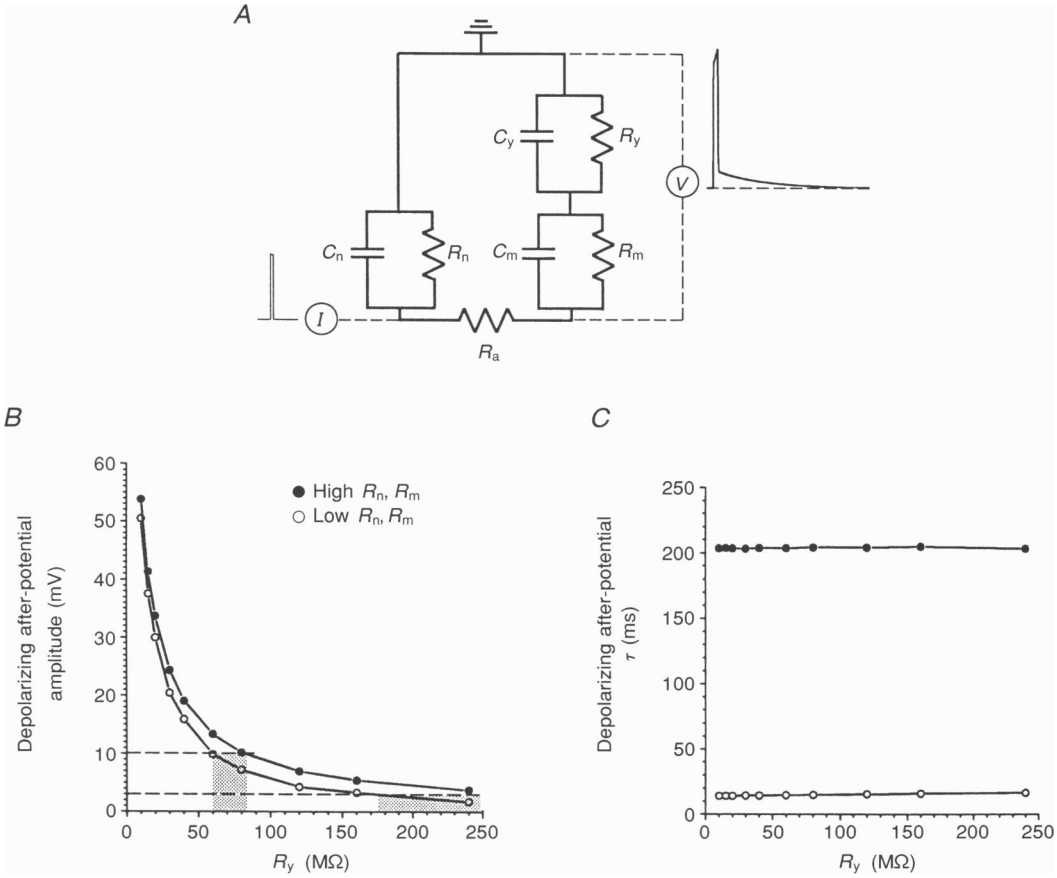

Figure 11. Simulated effects of myelin resistance (R_y) on the amplitude and time course of the depolarizing after-potential

A, simplified node–internode circuit used in simulations. *B*, simulated relationship between the peak amplitude of the depolarizing after-potential and R_y for minimal (○) and maximal (●) values of internodal (R_m) and nodal (R_n) resistances. Minimal values were 90 MΩ for R_m and 200 MΩ for R_n; maximal values were 1200 MΩ for R_m and 4000 MΩ for R_n. These values were calculated as described below in order to be compatible with the input resistances and passive time constants of decay measured in these axons. Shaded areas bracket the range of R_y compatible with the mean peak amplitudes of the depolarizing after-potentials measured in lizard and rat axons (10 and 3 mV, respectively, indicated by dashed lines). *C*, simulated relationship between the time constant of the depolarizing after-potential and R_y for minimal (○) and maximal (●) values of R_m and R_n. Simulations used an internodal axolemmal capacitance (C_m) of 0·22 nF, calculated assuming an axonal diameter of 7 μm, an internodal length of 1 mm, and a specific membrane capacitance of 1 μF cm^{-2}. Nodal capacitance (C_n) was 0·00022 nF (= 1/1000 C_m), and myelin sheath capacitance (C_y) was 0·0031 nF (= 1/70 C_m, assuming 35 myelin wraps × 2 membranes per wrap (Fig. 4) and a transmyelin leakage pathway as suggested by Blight, 1985). The resistance of the axoplasm, R_a, was calculated using a specific resistivity of 70 Ω cm. The action potential was simulated by injecting into the axon a current pulse sufficient to produce a 133 mV peak depolarization within 1·5 ms. The minimal R_n value (200 MΩ) was calculated using the input resistance (R_{in}) measured in hyperpolarized rat axons (around 30 MΩ, Fig. 5*C*), using the equation $R_t = (R_{in}^2\, \pi\, d^2)/R_a$, where R_t is the total (steady-state) resistance of the node in parallel with the (internode + myelin). For a 1 mm length of axon, R_t was 200 MΩ, which in this parallel circuit is also the minimum value for R_n. The minimum value for R_m (90 MΩ) was calculated from the time constant of decay of the passive voltage transient in hyperpolarized rat axons (about 20 ms, Fig. 5*E*); according to the passive charging model, during the depolarizing after-potential the internodal axolemmal capacitance charges through the internodal axolemma in parallel with the (node + myelin), and the minimal value of R_m in this circuit = time constant/C_m = 90 MΩ. The maximal value for R_m (1200 MΩ) was calculated by determining for the circuit shown in *A* all the R_n, R_m and R_y combinations compatible with the maximal input resistance (100 MΩ) and passive time constant (140 ms) measured in lizard axons, assuming a diameter of 7 μm. Maximal R_n was set at 4000 MΩ because simulations increasing R_n above this value yielded no further increase in depolarizing after-potential amplitude.

resistances of the nodal and internodal axolemmae of 7 μm diameter axons, as described in the figure legend. The amplitude of the simulated depolarizing after-potential decreased as R_y increased. As indicated by the shaded areas in Fig. 11*B*, for a depolarizing after-potential amplitude of 3 mV (the average for rat axons at the resting potential), the predicted value of R_y was 175 MΩ or greater, whereas for a depolarizing after-potential of 10 mV (the mean for lizard axons), the predicted R_y ranged from 61 to 83 MΩ. Assuming that R_y is proportional to myelin thickness, the measured ratio of rat : lizard myelin thickness of 1·1 : 0·87 = 1·15 (Fig. 4*D*) would account for at most 1–2 mV of the observed 7 mV difference between the mean peak amplitudes of their depolarizing after-potentials. Further simulations using this model (Fig. 11*C*) indicated that the slow time constant of decay of the depolarizing after-potential was relatively insensitive to R_y. These simulations therefore suggest that differences in myelin thickness (number of wraps) make no contribution to the different time courses of rat and lizard depolarizing after-potentials, and can account for only a fraction of the difference between their recorded amplitudes. Myelin-related factors might also contribute to the smaller amplitude of the depolarizing after-potential in rat axons if rat myelin had a higher resistance per unit thickness than lizard myelin, and/or if the myelin sheaths surrounding the finer branches of motor axons had a lower resistance in lizard than in rat axons.

Resting axolemmal resistance

Rat axons had a more rapidly decaying passive voltage response than lizard axons (Fig. 5). This faster time constant might result from a lower axolemmal capacitance and/or a lower resting axolemmal resistance. Assuming the passive charging model, a lower resting axolemmal resistance would better explain the observation that depolarizing after-potentials in rat axons had both a rapid decay and a small amplitude. (A lower capacitance would predict instead that rapidly-decaying depolarizing after-potentials would have large peak amplitudes, because smaller capacitances charge more rapidly.) Consistent with the idea that rats have a lower resting axolemmal resistance, rat axons had lower resting input resistances, and experiments in which K^+ was ionophoretically injected into the myelin sheath suggested greater resting activation of internodal axolemmal K^+ channels in rat than in lizard axons (David *et al.* 1992, 1993; Kapoor, Smith, Felts & Davies, 1993).

The finding that in both rat and lizard axons the rate of decay of the passive voltage response matched that of the depolarizing after-potential at hyperpolarized potentials (Fig. 5*E* and *F*) is consistent with the passive charging model for the depolarizing after-potential. However, for action potentials evoked at resting and depolarized potentials the depolarizing after-potential usually decayed more rapidly than the passive response. Possible reasons for this discrepancy, which was especially marked in rat axons, are that the passive charging model is incorrect, or that the action potential is followed by a persisting increase in a depolarization-activated axolemmal conductance that speeds the rate at which the charge on the internodal axolemmal capacitance returns to its resting value.

Persisting increase in axolemmal conductance(s) following action potentials

If the depolarizing after-potential is due to passive charging, then activation of axolemmal (especially internodal) K^+ conductances during or immediately following the action potential would reduce the amplitude of the depolarizing after-potential, by 'short-circuiting' the charging of the internodal axolemmal capacitance. If this conductance persisted, it would also speed the decay of the depolarizing after-potential.

Several lines of evidence suggest that a depolarization-activated K^+ conductance does indeed limit the peak amplitude of the depolarizing after-potential in both lizard and rat axons. First, during repetitive stimulation successive depolarizing after-potentials summated in axonal regions too hyperpolarized to discharge a full-sized action potential (Fig. 8), but showed little or no summation following full-amplitude action potentials (Figs 6–8; control records in Figs 9*C* and 10*B*). Second, in both lizard and rat axons the depolarization following the action potential increased following addition of K^+ channel blockers (Figs 9 and 10*A*, and Barrett *et al.* 1988). Part of this increase in depolarizing after-potential amplitude may have been due to prolongation of the action potential, with a consequent increase in the total depolarizing charge applied to the internodal axolemma. However, action potential prolongation does not account completely for effects of K^+ channel blockers on depolarizing after-potential amplitude, because Barrett *et al.* (1988) found that in lizard axons concentrations of TEA (10 mM) and 4-AP (1 mM) that produced similar increases in action potential duration (103 and 92%, respectively) produced markedly different increases in the peak amplitude of the slow component of the depolarizing after-potential (155 and 16%, respectively). At least some of the axolemmal K^+ channels activated following action potentials are internodal (David *et al.* 1992, 1993; Kapoor *et al.* 1993).

How long do depolarization-activated axolemmal K^+ channels remain activated following the action potential? In rat axons several observations suggest that this activation persisted for at least 50 ms. First, the depolarizing after-potential decayed much more rapidly than the passive voltage response at resting and depolarized membrane potentials (Fig. 5*E*). The discrepancy between these curves provides an upper limit to the contribution of K^+ channel activation to the time course of the depolarizing after-potential. Second, during repetitive stimulation the interspike voltage trajectory became

progressively more hyperpolarized (Figs 6 and 9*C*), and both single spikes and trains were followed by a prolonged hyperpolarizing after-potential (Figs 1*B* and 9*B*) attributed to a TEA-sensitive K^+ conductance (Baker *et al.* 1987; Eng *et al.* 1988). In lizard axons the persisting K^+ conductance was probably less prominent than in rat axons, because the discrepancy between the rates of decay of the depolarizing after-potential and the passive voltage transient at resting and depolarized potentials was less marked than in rat axons (compare *E* and *F* in Fig. 5). Also, the voltage response to a hyperpolarizing current pulse injected during the first depolarizing after-potential in a train was similar to that measured in the resting axon (compare Fig. 7*C* and *D*). Nonetheless, lizard axons evidenced progressive activation of a persisting conductance because during repetitive stimulation the depolarizing after-potential following full-sized action potentials showed little or no summation (Figs 6, 7*A*, 8 and 10*B*), and current injections demonstrated an increased input conductance during later interspike intervals (compare Fig. 7*C* and *D*).

The identity of the K^+ channels that modify the depolarizing after-potential in rat and lizard axons remains uncertain, but we hypothesize that the S and I (or f_1) types of delayed-rectifier channnel play important roles, because of their voltage ranges of activation, rates of deactivation and pharmacology. S-type delayed-rectifier channels, identified in nodal and paranodal membranes of rat axons and in nodal and internodal membranes of frog axons, begin activating at potentials hyperpolarized to rest and deactivate over hundreds of milliseconds; I-type delayed-rectifier channels activate over the range −80 to −30 mV and inactivate over tens of milliseconds (Dubois, 1981; Grissmer, 1986; Röper & Schwarz, 1989; Safronov *et al.* 1993). TEA, which blocks both S- and I-type channels, increased both early and late components of the depolarizing after-potential in lizard axons (Fig. 10 and Barrett *et al.* 1988), and aminopyridines, which block I- but not S-type channels, especially enhanced the earlier portions of the depolarizing after-potential (Figs 9 and 10). F (or f_2)-type delayed-rectifier channels probably have little effect on the time course of the depolarizing after-potential, since they activate only at voltages depolarized to −50 mV and deactivate within a few millseconds (Dubois, 1981; Safronov *et al.* 1993). The high intracellular Na^+ concentrations required to activate Na^+-activated K^+ channels (33 mM for half-maximal activation; Koh *et al.* 1994) would most probably be achieved only near nodes following intense stimulation. Present evidence suggests that Ca^{2+}-activated K^+ channels make little contribution to axonal after-potentials in physiological saline because depolarizing and hyperpolarizing after-potentials are not blocked by Mn^{2+} or by Ca^{2+}-free solutions (Barrett & Barrett, 1982; Eng *et al.* 1988).

Combined with previously published work, the experimental and modelling results presented here suggest that the peak amplitude of the depolarizing after-potential in myelinated axons decreases as myelin resistance increases and/or as axolemmal (especially internodal) K^+ channels become activated. The rate of decay of the depolarizing after-potential increases as axolemmal conductance increases. The hypothesis that the depolarizing after-potential is mediated by charging of the internodal axolemma must be modified to take into account axolemmal K^+ conductances that remain activated following the action potential. These conductances, at least some of which are internodal, appear to be more prominent in rat than in lizard axons.

Angaut-Petit, D., Benoit, E. & Mallart, A. (1989). Membrane currents in lizard motor nerve terminals and nodes of Ranvier. *Pflügers Archiv* **415**, 81–87.

Baker, M., Bostock, H., Grafe, P. & Martius, P. (1987). Function and distribution of three types of rectifying channel in rat spinal root myelinated axons. *Journal of Physiology* **383**, 45–67.

Barrett, E. F. & Barrett, J. N. (1982). Intracellular recording from vertebrate myelinated axons: mechanism of the depolarizing after-potential. *Journal of Physiology* **323**, 117–144.

Barrett, E. F., Morita, K. & Scappaticci, K. A. (1988). Effects of tetraethylammonium on the depolarizing after-potential and passive properties of lizard myelinated axons. *Journal of Physiology* **402**, 65–78.

Blight, A. R. (1985). Computer simulation of action potentials and afterpotentials in mammalian myelinated axons: the case for a lower resistance myelin sheath. *Neuroscience* **15**, 13–31.

Blight, A. R. & Someya, S. (1985). Depolarizing afterpotentials in myelinated axons of mammalian spinal cord. *Neuroscience* **15**, 1–12.

Bowe, C. M., Kocsis, J. D. & Waxman, S. G. (1987). The association of the supernormal period and the depolarizing afterpotential in myelinated frog and rat sciatic nerve. *Neuroscience* **21**, 585–593.

Chiu, S. Y. & Ritchie, J. M. (1980). Potassium channels in nodal and internodal axonal membrane of mammalian myelinated fibres. *Nature* **284**, 170–171.

Chiu, S. Y. & Ritchie, J. M. (1981). Evidence for the presence of potassium channels in the paranodal region of acutely demyelinated mammalian single nerve fibres. *Journal of Physiology* **313**, 415–437.

Chiu, S. Y. & Ritchie, J. M. (1982). Evidence for the presence of potassium channels in the internode of frog myelinated nerve fibres. *Journal of Physiology* **322**, 485–501.

Chiu, S. Y. & Schwarz, W. (1987). Sodium and potassium currents in acutely demyelinated internodes of rabbit sciatic nerves. *Journal of Physiology* **391**, 631–649.

Chiu, S. Y., Shrager, P. & Ritchie, J. M. (1985). Loose patch clamp recording of ionic currents in demyelinated frog nerve fibers. *Brain Research* **359**, 338–342.

David, G., Barrett, J. N. & Barrett, E. F. (1992). Evidence that action potentials activate an internodal potassium conductance in lizard myelinated axons. *Journal of Physiology* **445**, 277–301.

David, G., Barrett, J. N. & Barrett, E. F. (1993). Activation of internodal potassium conductance in rat myelinated axons. *Journal of Physiology* **472**, 177–202.

Dubois, J. M. (1981). Evidence for the existence of three types of potassium channels in the frog Ranvier node membrane. *Journal of Physiology* **318**, 297–316.

Eng, D. L., Gordon, T. R., Kocsis, J. D. & Waxman, S. G. (1988). Development of 4-AP and TEA sensitivities in mammalian myelinated nerve fibers. *Journal of Neurophysiology* **60**, 2168–2179.

Friede, R. L. & Samorajski, T. (1967). Relation between the number of myelin lamellae and axon circumference in fibers of vagus and sciatic nerves of mice. *Journal of Comparative Neurology* **130**, 223–232.

Gasser, H. S. (1935). Changes in nerve-potentials produced by rapidly repeated stimuli and their relation to the responsiveness of nerve to stimulation. *American Journal of Physiology* **111**, 35–50.

Gasser, H. S. & Erlanger, J. (1930). The ending of the action potential and its relation to other events in nerve activity. *American Journal of Physiology* **94**, 247–277.

Gasser, H. S. & Grundfest, H. (1936). Action and excitability in mammalian A fibres. *American Journal of Physiology* **117**, 113–133.

Glantz, S. A. & Slinker, B. K. (1990). *Primer of Applied Regression and Analysis of Variance*. McGraw-Hill, New York.

Grissmer, S. (1986). Properties of potassium and sodium channels in frog internode. *Journal of Physiology* **381**, 119–134.

Hildebrand, C. (1971). Ultrastructural and light-microscopic studies of the developing feline spinal cord white matter. I. The nodes of Ranvier. *Acta Physiologica Scandinavica*, suppl. 364, 81–97.

Jonas, P., Bräu, M. E., Hermsteiner, M. & Vogel, W. (1989). Single-channel recording in myelinated nerve fibers reveals one type of Na channel but different K channels. *Proceedings of the National Academy of Sciences of the USA* **86**, 7238–7242.

Jonas, P., Koh, D.-S., Kampe, K., Hermsteiner, M. & Vogel, W. (1991). ATP-sensitive and Ca-activated K channels in vertebrate axons: novel links between metabolism and excitability. *Pflügers Archiv* **418**, 68–73.

Kapoor, R., Smith, K. J., Felts, P. A. & Davies, M. (1993). Internodal potassium currents can generate ectopic impulses in mammalian myelinated axons. *Brain Research* **611**, 165–169.

Kirschner, D. A., Ganser, A. L. & Caspar, D. L. D. (1984). Diffraction studies of molecular organization and membrane interactions in myelin. In *Myelin*, ed. Morell, P., pp. 51–95 Plenum Press, New York.

Kocsis, J. D. & Waxman, S. G. (1981). Action potential electrogenesis in mammalian central axons. In *Advances in Neurology*, vol. 31, *Demyelinating Diseases, Basic and Clinical Electrophysiology*, ed. Waxman, S. G. & Ritchie, J. M., pp. 299–312. Raven Press, New York.

Koh, D.-S., Jonas, P., Bräu, M. E. & Vogel, W. (1992). A TEA-insensitive flickering potassium channel active around the resting potential in myelinated nerve. *Journal of Membrane Biology* **130**, 149–162.

Koh, D.-S., Jonas, P. & Vogel, W. (1994). Na^+-activated K^+ channels localized in the nodal region of myelinated axons of *Xenopus*. *Journal of Physiology* **479**, 183–197.

Morita, K. & Barrett, E. F. (1989). Calcium-dependent depolarizations originating in lizard motor nerve terminals. *Journal of Neuroscience* **9**, 3359–3369.

Morita, K., Barrett, E. & Katayama, Y. (1990). Membrane potential oscillations in tetraethylammonium-treated peripheral myelinated axons. *Neuroscience Research Supplement* **11**, S121.

Morita, K., David, G., Barrett, J. N. & Barrett, E. F. (1993). Posttetanic hyperpolarization produced by electrogenic Na^+-K^+ pump in lizard axons impaled near their motor terminals. *Journal of Neurophysiology* **70**, 1874–1884.

Peters, A., Palay, S. L. & Webster, H. F. (1991). *The Fine Structure of the Nervous System: Neurons and Their Supporting Cells*, 3rd edn, p. 224. Oxford University Press, New York.

Quick, D. C., Kennedy, W. R. & Donaldson, L. (1979). Dimensions of myelinated nerve fibers near the motor and sensory terminals in cat tenuissimus muscles. *Neuroscience* **4**, 1089–1096.

Röper, J. & Schwarz, J. R. (1989). Heterogeneous distribution of fast and slow potassium channels in myelinated nerve fibres. *Journal of Physiology* **416**, 93–110.

Safronov, B. V., Kampe, K. & Vogel, W. (1993). Single voltage-dependent potassium channels in rat peripheral nerve membrane. *Journal of Physiology* **460**, 675–691.

Williams, P. L. & Wendell-Smith, C. P. (1960). The use of fixed and stained sections in quantitative studies of peripheral nerve. *Quarterly Journal of Microscopical Science* **101**, 43–54.

Wilson, G. F. & Chiu, S. Y. (1990). Ion channels in axon and Schwann cell membranes at paranodes of mammalian myelinated fibers studied with patch clamp. *Journal of Neuroscience* **10**, 3263–3274.

Wu, J. V., Rubinstein, C. T. & Shrager, P. (1993). Single channel characterization of multiple types of potassium channels in demyelinated *Xenopus* axons. *Journal of Neuroscience* **13**, 5153–5163.

Acknowledgements

We thank Dr Kenneth Muller for extensive help with the electron micrographs, and Dr Wolfgang Nonner for reading a preliminary version of the manuscript. This was supported by NS 12404 from the National Institutes of Health, a Muscular Dystrophy Association postdoctoral fellowship to K.A.S. and an NIMH postdoctoral fellowship to B.M.

Authors' present addresses

B. Modney: Department of Biology, Cleveland State University, 2399 Euclid Avenue, Cleveland, OH 44115, USA.

K. A. Scappaticci: Pfizer, Inc., 235 East 42nd Street, Room 219/4/4, New York, NY 10017, USA.

Received 4 January 1995; accepted 17 May 1995.